



Reactive spontaneous infiltration of Al-activated TiO₂ by molten aluminum

Abdollah SABOORI¹, Xiang CHEN^{1,2}, Claudio BADINI¹, Paolo FINO¹, Matteo PAVESE¹

1. Department of Applied Science and Technology, Politecnico di Torino,
Corso Duca Degli Abruzzi 24, 10129 Torino, Italy;

2. Research Center of Graphene Applications, Beijing Institute of Aeronautical Materials, Beijing 100095, China

Received 6 May 2018; accepted 12 October 2018

Abstract: The reactive spontaneous infiltration of Al-activated TiO₂ (anatase) was investigated. Pure Al powder was blended with TiO₂ for activation. They were compacted into the preform and then sealed within 6060 alloy mould. The activation and infiltration were carried out in 6060 alloy bath for 1 h and comparative sintering experiments were carried out in an argon protected environment under the same conditions of temperature and duration. X-ray diffraction analysis proved that the Al sealed environment was superior to the argon protection on activating the reaction between Al and TiO₂. The blending ratio of TiO₂ to Al and the temperature were found to play the most important role in infiltration by affecting infiltration and reaction kinetics. Three main types of microstructures were observed after infiltration: full infiltration, partial infiltration with the formation of cracks and no infiltration. The formation of these microstructures was explained on the basis of reaction kinetics and local volume changes due to the reactions. Ultimately, it is found that to obtain an overall good spontaneous infiltration, a TiO₂ to Al blending ratio around 3:7 in volume and an infiltration temperature around 900 °C are the most suitable.

Key words: spontaneous infiltration; pressureless sintering; TiO₂–Al reaction; infiltration kinetics; in-situ fabrication

1 Introduction

With the progress of technology, more challenges of course will be raised for different industries, such as automotive, aerospace and electro-packaging industries [1]. For instance, according to new environmental rules, automotive industries should change their strategies to produce vehicles with lower CO₂ emission. One of the solutions is changing the design of components which are used in the vehicles to reduce their weight and maintain even improve their mechanical properties. However, the parts with new complex designs cannot be produced by conventional technologies and require new production technologies like additive manufacturing (AM) technologies. In fact, by AM technologies, it would be possible to produce any complex shape and fulfill the required criteria [2,3]. Nonetheless, since this technology is recently developed, several efforts should be undertaken to reduce the cost of production. Another solution that can address the future challenges is materials development which is more economical and easier than technology development.

The wide application of aluminum in the automotive and aerospace industry, makes aluminum-matrix composites an important option to meet future challenges in the design of structural components. In this concern, the reinforcement material used in the production of composites plays a key role in order to maximize the mechanical performance of the composites [4–8]. The use of nanometric reinforcement materials for the development of aluminum-matrix composites has demonstrated a positive effect on the mechanical behavior of the final products [9].

Metal matrix nanocomposites (MMNCs) reinforced by nanoparticles has been developed over last decades and gradually formed an important part in materials selection for aeronautic, automotive, defense and electro packaging industries [10–14]. In recent years, there has been an increasing interest in the development of new composite materials and fabrication techniques [15–18]. In-situ composites are multiphase materials where the reinforcing phases are synthesized within the matrix during composite fabrication [19]. Due to the formation of ultrafine and thermal-stable ceramic or intermetallic reinforcements, the in-situ composites present excellent

mechanical properties [20]. Together with the development of various fabrication techniques, in-situ composites have been attracting considerable attention over the last thirty years.

TiO₂-Al is an interesting material system where the products are tailorable by controlling the ratio between starting reagents [21], i.e.,



Al₂O₃ together with one or several intermetallic phases (Ti₃Al, TiAl and TiAl₃) and titanium oxides phases (Ti₂O, TiO, Ti₂O₃, Ti₃O₅, etc.) have been observed after TiO₂-Al reactions [22]. In this system, several approaches, such as self-propagating high-temperature synthesis (SHS) [23], reactive hot pressing (RHP) [24], reactive infiltration [25,26], have been tested and demonstrated to be feasible for preparing in-situ composites. For example, HORVITZ et al [24] fabricated an Al₂O₃-Ti aluminide interpenetrating composite from a compacted 3TiO₂-7Al powder blend by SHS and RHP techniques; PENG et al [27,28] fabricated TiAl₃-Al₂O₃-Al in-situ composites through squeeze casting route. Among all the approaches, reactive infiltration method is most commonly investigated in the literatures, and the standard processing comprises the pressure infiltration of Al into TiO₂ preform followed by a further reactive heat-treatment. For instance, PAN et al [29] reported a TiAl₃-Al₂O₃-Al composite by squeeze casting Al into anatase TiO₂ whiskers and then heat treating. WAGNER et al [30] fabricated an interpenetrating Al₂O₃-TiAl₃ composite by infiltrating Al into sintered TiO₂-containing Al₂O₃ preforms, followed by annealing for 4 h in air at 640 °C. However, owing to the volume shrinkage of the products during the annealing treatment, porosity develops between the in-situ formed products, which worsens the composite performance in many aspects. One possible solution to overcome these problems and to avoid the need for high pressure is to develop spontaneous infiltration techniques, where infiltration is carried out along with the reactions, and hence the porosities formed by the shrinkage are filled simultaneously during the infiltration. However, little attention has been paid to the reactive spontaneous infiltration of TiO₂-Al and less research progress has been reported in this field.

This work presents a study on the reactive spontaneous infiltration of TiO₂-Al. Some phenomena related to the kinetics of reaction and infiltration are revealed and investigated, and the influence of some key parameters is discussed.

2 Experimental

In-situ TiAl₃-Al₂O₃-Al composites were fabricated by the reactive spontaneous infiltration technology. The

processing steps comprised TiO₂-Al mixture preparation, preform forming, sealing into Al alloy molds and pressureless infiltration. Anatase TiO₂ powders (<45 μm, from Sigma Aldrich) and Al powders (<45 μm, from Alfa Aesar) were used as starting materials in the present work. 6060 aluminum alloy (from CO.ME.F.I. Metalli srl) was used to prepare the molds for sealing and served also as infiltration bath after melting.

Anatase TiO₂ and Al powders were mixed by stirring in ethanol and then dried by heating. The blending ratios were 3:7, 1:1 and 7:3 in volume, which corresponded to TiO₂-70vol.%Al, TiO₂-50vol.%Al and TiO₂-30vol.%Al, respectively. These mixtures were compacted into cylinder-shape preforms with diameters of 10 and 12 mm, respectively, through unidirectional cold pressing under a pressure of 175 MPa. The d_{12} mm preforms were placed and sealed into 6060 aluminum molds for further pressureless infiltration treatment, while the d_{10} mm preforms were used for pressureless sintering treatment as comparison. In the pressureless infiltration treatment, the sealed preforms were treated in a fast heating furnace (Bicasa). They were heated to the required temperature (800, 900 and 1000 °C) at 300 °C/h and then kept at that temperature for 1 h. After furnace cooling, they were taken out directly from the molten Al bath at 700 °C and further cooled to room temperature in air. In the pressureless sintering treatment, the d_{10} mm preforms were placed in a furnace working under argon protection, heated to the required temperature (800, 900 and 1000 °C) at 300 °C/h and kept for 1 h. Afterwards they were cooled to room temperature inside the furnace. The schematics of experimental processes are shown in Figs. 1(a) and (b).

The treated specimens were cut, and the morphology and phase composition were analyzed by optical microscopy and X-ray diffractometry, respectively. To study the microstructure of specimens by an optical microscope (OM), they were mounted in resin and ground with SiC papers down to 4000 grit size and thereafter by diamond paste (down to 1 μm) [31,32]. The panoramas of the cross sections were stitched from at least 100 photos.

X-ray diffraction (XRD) patterns of as-polished samples were recorded on a Philips X'Pert diffractometer using Cu K_α radiation. Sample preparation for XRD analysis included grinding the samples with the height of less than 5 mm down to 4000 grit size SiC paper, washing and drying.

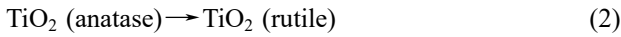
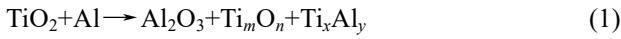
3 Results and discussion

3.1 Reaction mechanism

The XRD patterns of TiO₂-70vol.%Al samples, both sintered and infiltrated in a temperature range of

800–1000 °C are presented in Fig. 2. As a reference, the XRD pattern of a green preform from TiO₂-70vol.%Al mixture is also given in the figure. The starting preform displayed the specific peaks of Al and anatase as expected. The change in the peaks intensity and the appearance of new peaks reveal that some reactions took place during various sintering and infiltration processes.

For the sample sintered at 800 °C, some low-intensity peaks of rutile, α-Al₂O₃, TiAl₃ and Ti_mO_n (titanium oxides with lower oxygen content than TiO₂, such as Ti₃O₅, Ti₂O₃, TiO and Ti₂O) appeared, along with the weakening of the peak-intensity of anatase phase. This indicates that during the reactive sintering at 800 °C, two phenomena took place, a reaction between Al and TiO₂ (Reaction 1) and the phase transformation of anatase into rutile (Reaction 2).



However, these reactions were relatively mild, because anatase and Al phases still co-existed after 1 h of

sintering at 800 °C.

At the higher sintering temperature of 900 °C, anatase, rutile, Ti_mO_n, α-Al₂O₃, TiAl₃ and Al phases were identified. The result is very similar to the case of sintering at 800 °C, except that the intensity of anatase is much lower and that of Al₂O₃ and TiAl₃ is much higher.

After sintering at 1000 °C, the starting anatase and Al phases were almost completely consumed after 1 h, because they were converted into the final products of α-Al₂O₃ and TiAl₃ according to the following equation:



From the above XRD phase analysis of sintered TiO₂-70vol.%Al specimens, it can be concluded that above 800 °C anatase converts into the more stable rutile phase, and that the reactions between TiO₂ and Al lead to the formation of transitional Ti_mO_n phases (such as Ti₃O₅, Ti₂O₃, TiO and Ti₂O) at low temperature. At higher temperature, the reaction forms mainly Al₂O₃ and TiAl₃, with the kinetics of the reaction increasing with temperature.

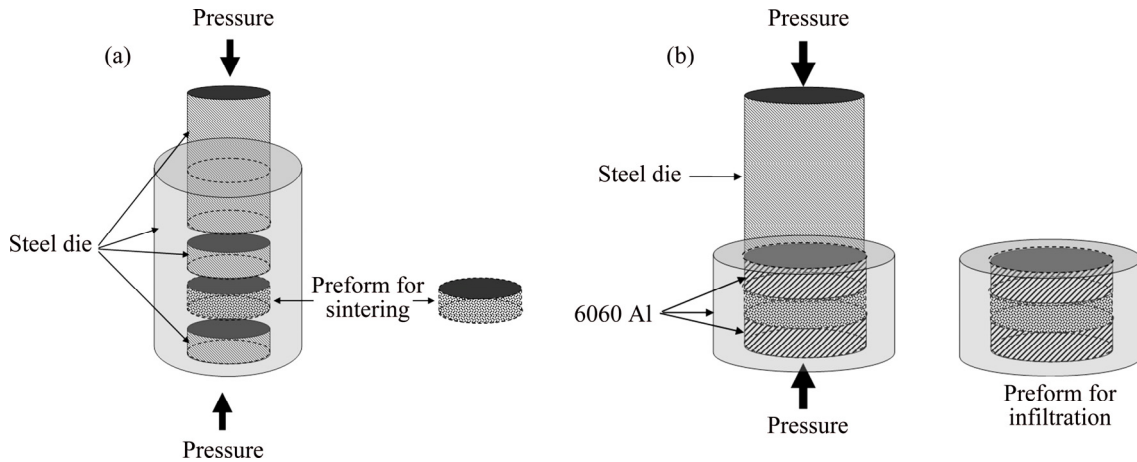


Fig. 1 Schematics of experimental processes: (a) Preform preparation for sintering; (b) Preform preparation for infiltration

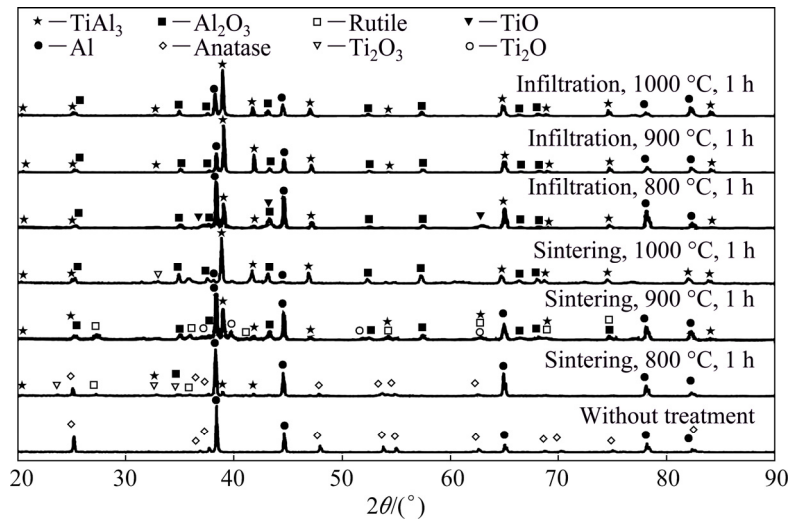


Fig. 2 XRD patterns of TiO₂-70vol.%Al specimens with different treatments

In the cases of infiltrated TiO_2 -70vol.%Al specimens, similar transitional Ti_mO_n phases were detected as well at low temperature, while no rutile was observed. At 800 °C, the peaks of TiO_2 (both anatase and rutile) were not present anymore, while TiAl_3 had higher peak intensity compared to the case of sintered specimens, and only small peaks of the transitional Ti_mO_n phases were observed in the pattern. At 900 and 1000 °C, the patterns were very similar, which indicates that complete reaction took place. Excess Al was observed in these two specimens, which probably came from the external Al bath during infiltration.

Figures 3 and 4 exhibit the XRD patterns of TiO_2 -50vol.%Al and TiO_2 -30vol.%Al samples, respectively. Similar phase analysis was carried out as in Fig. 2, and the results are summarized in Table 1.

By reducing the aluminum content, there is a clear increase in the transitional Ti_mO_n phases quantity, and also some TiAl_2 intermetallic forms. Moreover, the

reaction seems less intense than in the aluminum-rich compositions. This is reasonable since for the Reaction (3) a theoretical volume ratio between TiO_2 and Al of 2:3 is expected, corresponding to 60 vol.% Al. Thus, at least for the sintering case, where no additional Al can sustain the reaction, the presence of partially reacted phases is expected.

The comparison between sintered and infiltrated samples shows that the intensity of the TiO_2 -Al reaction is higher in the infiltration cases (with the same blending ratio and heat treating temperature). This is probably due to the fact that in the infiltration case extra Al has accessed to the reacting mixture, and lower oxygen partial pressure is experienced during the infiltration, thanks to the sealing effect of the liquid Al alloy bath. The access of extra Al could increase the contact area with TiO_2 phase, and thus promote the reaction. Oxygen partial pressure could modify the thickness of the aluminum oxide layer surrounding the Al powders and

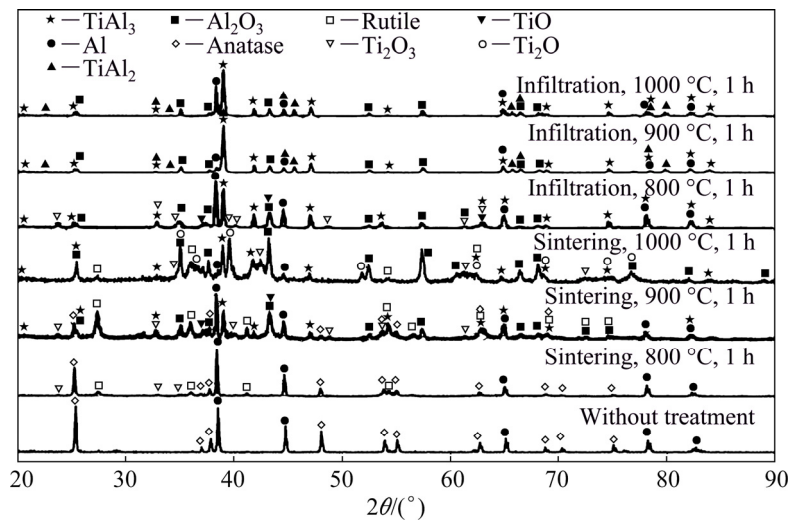


Fig. 3 XRD patterns of TiO_2 -50vol.%Al specimens with different treatments

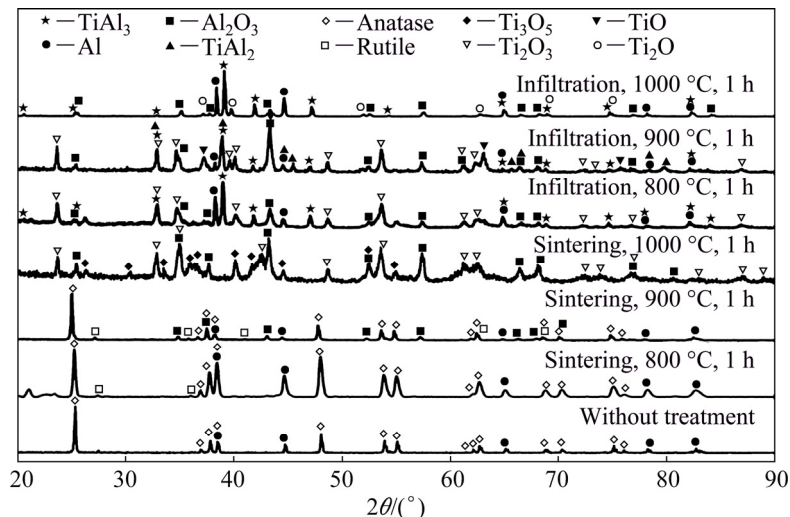


Fig. 4 XRD patterns of TiO_2 -30vol.%Al specimens with different treatments

Table 1 Phase composition of various specimens

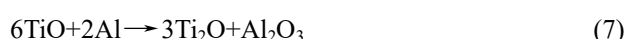
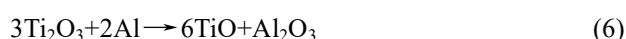
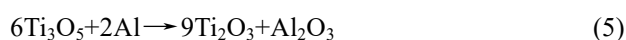
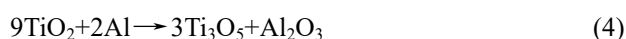
Method	Temperature/ °C	TiO ₂ -70vol.%Al	TiO ₂ -50vol.%Al	TiO ₂ -30vol.%Al
Green preform		Anatase, Al	Anatase, Al	Anatase, Al
Sintering	800	Anatase, Al , rutile, TiAl ₃ , Ti _m O _n , Al ₂ O ₃	Anatase, Al , rutile, Ti _m O _n , Al ₂ O ₃	–
	900	TiAl₃, Al , rutile, Ti _m O _n , Al ₂ O ₃	TiAl₃, Al, Al₂O₃, rutile , Ti _m O _n	Anatase, Al, Al₂O₃ , rutile
	1000	TiAl₃, Al₂O₃ , Al, Ti _m O _n	TiAl₃, Al₂O₃, Ti_mO_n , Al	Al₂O₃, Ti_mO_n
Infiltration	800	TiAl₃, Al , Ti _m O _n , Al ₂ O ₃	TiAl₃, Al , Ti _m O _n , Al ₂ O ₃	TiAl₃, Al , Ti _m O _n , Al ₂ O ₃
	900	TiAl₃, Al, Al₂O₃	TiAl₃, TiAl₂ , Al, Al ₂ O ₃	TiAl₃, TiAl₂, Al₂O₃, Ti_mO_n , Al
	1000	TiAl₃, Al, Al₂O₃	TiAl₃, TiAl₂ , Al, Al ₂ O ₃	TiAl₃, Al , Ti _m O _n , Al ₂ O ₃

The phases in bold are the major phases, and the rests are the minor phases

affect the spreading of liquid Al over the TiO₂ phase. In the sintering cases, specimens were protected by high purity argon ($\approx 1 \times 10^{-7}$ of oxygen), so that the oxygen partial pressure was calculated to be around 1×10^{-2} Pa, considerably higher than the critical oxidation pressure of Al (for instance 1×10^{-35} Pa at 900 °C and 1×10^{-29} Pa at 1200 °C). Therefore, a sufficiently thick and dense aluminum oxide layer would form on the surface of Al phase to slow further oxidation. Instead, in the infiltration case, specimens were arranged in a closed environment (sealed by Al bath), and the oxygen in the sealed space would be gradually consumed until some equilibrium is reached (e.g., oxidation and reduction). In this way, an extremely low value of PO₂ is probably achieved and the thickness of surface aluminum oxide layer is therefore reduced.

Besides, the raising in temperature can effectively increase the diffusion ability and critical oxidation pressure of Al. This would lead again to the reduction of the thickness of the surface aluminum oxide and bring faster Al diffusion over the oxide layer. Therefore, raising temperature can also enhance the reaction kinetics between TiO₂ and Al.

As suggested by CHEN et al [33], the reduction of TiO₂ by Al is a stepwise process, which is likely to occur, from the perspective of thermodynamics, according to the following sequences:



In the temperature range of 800–1000 °C, the reaction thermodynamics are much the same in both the sintering and infiltration treatments. Thus, it seems only a matter of time to obtain complete reaction products, provided that sufficient Al is available. However, the

products would be further affected by various phenomena involved, for instance, the mass transfer and the chemical or physical changes during reactive sintering of TiO₂-Al.

3.2 Morphology

Figure 5 presents the cross-sectional panoramas of specimens of TiO₂-70vol.%Al, TiO₂-50vol.%Al and TiO₂-30vol.%Al sintered for 1 h at 800, 900 and 1000 °C, respectively. Each of these images was obtained by stitching at least 100 micrographs. Despite the specimens sintered at 800 °C were too fragile to be polished, the main features of these cross section were still distinguishable. One of the common features of the sintered specimens is the appearance of annular layers, which is most evident in the specimen sintered at 1000 °C with a TiO₂-to-Al blending ratio of 1:1 (Fig. 5(b₃)). The annular layers were formed probably by the combustion waves induced from TiO₂-Al reactions, while the involved complex movement of liquid Al phase resulted in the individual microstructure of the single specimen types. For instance, when Al phase is abundant, the tendency for liquid Al phase to converge in the center is evident, probably in order to lower its surface energy, bringing to a “central-gathering” microstructure, where the pores of the preform are filled in the central area, leaving the external zone of the specimens poor in aluminum (Fig. 5(a)). When Al phase is not sufficient to get the full reaction, but still present in rather high quantity, liquid Al phase can only gather in short range at some local area with better wettability (e.g., at some combustion wave front where a higher temperature is observed); this phenomenon leads to the “annular-gathering” microstructure, where alternated Al-rich and Al-poor rings are observed (Fig. 5(b)). When the quantity of Al phase is very low, liquid Al phase can hardly flow anywhere, and no evident annular layer is observed in TiO₂-30vol.%Al specimens (Fig. 5(c)).

Another common feature in the sintered specimens is the presence of cracks. Two typical forms of cracks are

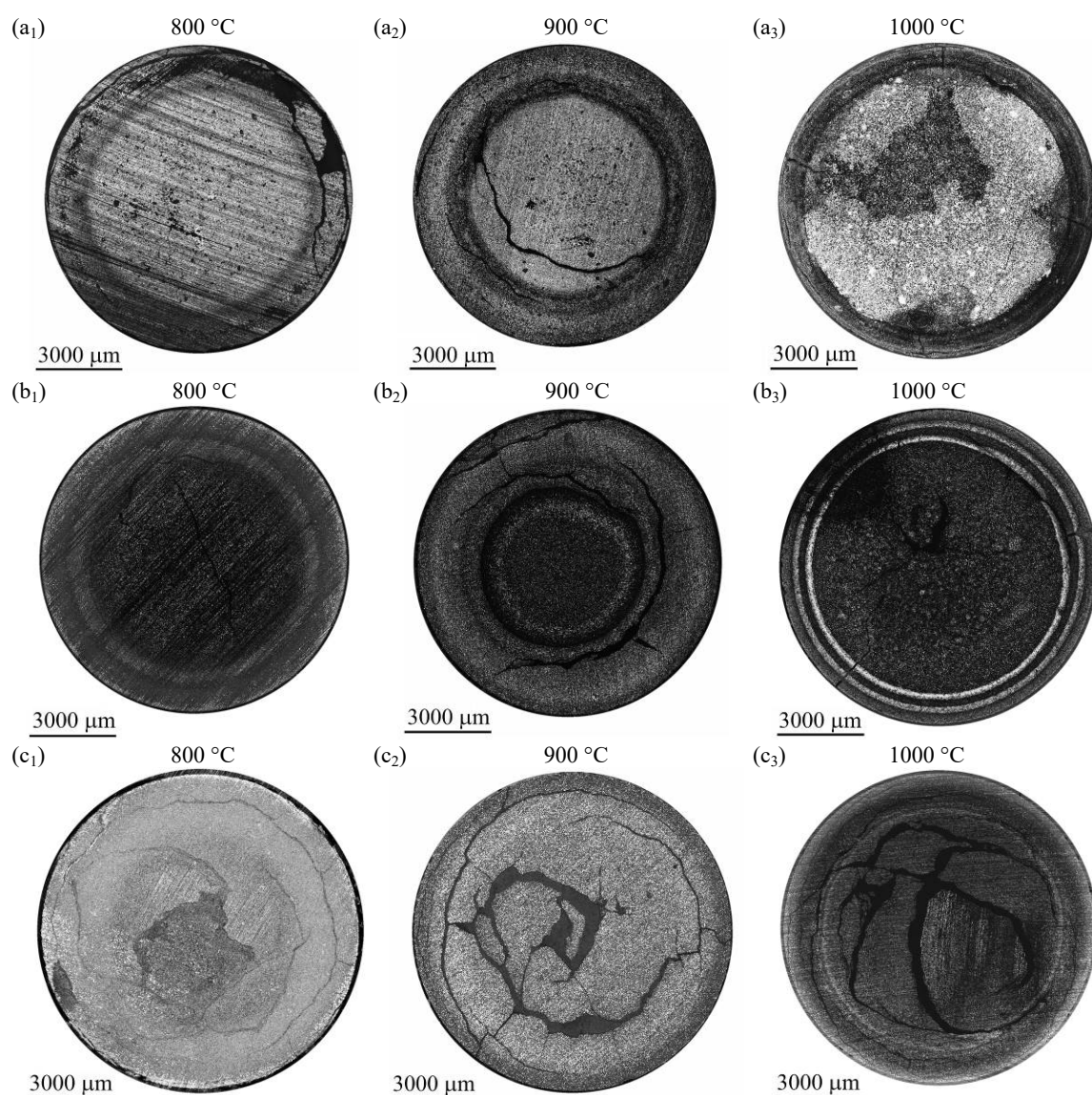


Fig. 5 Cross-sectional panoramas of sintered specimens: (a) TiO_2 -70vol.%Al; (b) TiO_2 -50vol.%Al; (c) TiO_2 -30vol.%Al

shown in the images: one is a uniform cracking within the entire specimen (Fig. 5(c)), and the other is the radial cracking that starts from the exterior (Fig. 5(a₃) and Fig. 5(b₃)). Volume variation is one major reason for these cracks, that comes from two aspects: the first is the volume shrinkage from anatase (3.9 g/cm^3) to rutile (4.2 g/cm^3) phase, and the other is the TiO_2 -Al reaction. The volume variations in various steps of the reaction can be evaluated in Reactions (3), (4), (9) and (10):



Generally, there is a reduction in the total volume after the possible reactions take place between TiO_2 and Al, as shown in Table 2 (the following density data are applied in the calculation, in g/cm^3 : TiO_2 , 3.9; Al, 2.7; Ti_3O_5 , 4.9; Ti_2O_3 , 4.5; TiO, 5.0; TiAl_3 , 3.3; Al_2O_3 , 3.9). This increases the porosity in the sintered specimens. On

the other hand, the volume of solid phases greatly increases, especially when TiAl_3 is formed, and this can generate cracks in the specimen. Thus, the uniform cracking is probably caused by a homogeneous volume shrinkage within the specimens, while the radial cracking is probably due to a local, severe and incongruous volume variation of the solid phases during the reactions.

Figure 6 exhibits the cross-sectional panoramas of specimens of TiO_2 -70vol.%Al, TiO_2 -50vol.%Al and TiO_2 -30vol.%Al infiltrated for 1 h at 800, 900 and 1000 °C, respectively. The microstructures are quite different from the corresponding cases of sintering, with fewer cracks and pores, thanks to the infiltration of liquid aluminum from the infiltration bath.

When being compared to the sintered TiO_2 -70vol.%Al specimens, the appearance of the infiltrated TiO_2 -70vol.%Al ones demonstrated that a successful infiltration took place. The structure is homogeneous,

and aluminum can be found all around the specimens, as shown in Fig. 5(a). However, as shown previously by XRD phase analysis, only the TiO_2 -70vol.%Al specimens infiltrated at 900 and 1000 °C for 1 h are completely reacted, while the ones infiltrated at 800 °C still contain transitional Ti_mO_n phases.

The case of the sample of TiO_2 -50vol.%Al infiltrated at 800 °C for 1 h (Fig. 6(b₁)) is similar to the previous ones, since a homogeneous structure is observed, demonstrating a successful infiltration of the Al-TiO₂ compact by the liquid aluminum alloy. Instead, the TiO_2 -50vol.%Al specimens infiltrated at the higher

Table 2 Evaluation of volume variation in reactions between TiO_2 and Al

Reaction	Reactant	Volume of reactions/cm ³	Product	Volume of products/cm ³	Volume variation rate/%	
					In total	In solid phase
(4)	9TiO ₂ (s)	184.6	3Ti ₃ O ₅ (s)	137.1	-20.2	-11.5
	2Al (l)	20.0	Al ₂ O ₃ (s)	26.2		
(9)	6TiO ₂ (s)	123.1	3Ti ₂ O ₃ (s)	96.0	-14.6	-0.7
	2Al (l)	20.0	Al ₂ O ₃ (s)	26.2		
(10)	3TiO ₂ (s)	61.5	3TiO (s)	38.4	-20.7	5.0
	2Al (l)	20.0	Al ₂ O ₃ (s)	26.2		
(3)	3TiO ₂ (s)	61.5	3TiAl ₃ (s)	117.3	-11.4	175.8
	13Al (l)	130.0	2Al ₂ O ₃ (s)	52.3		

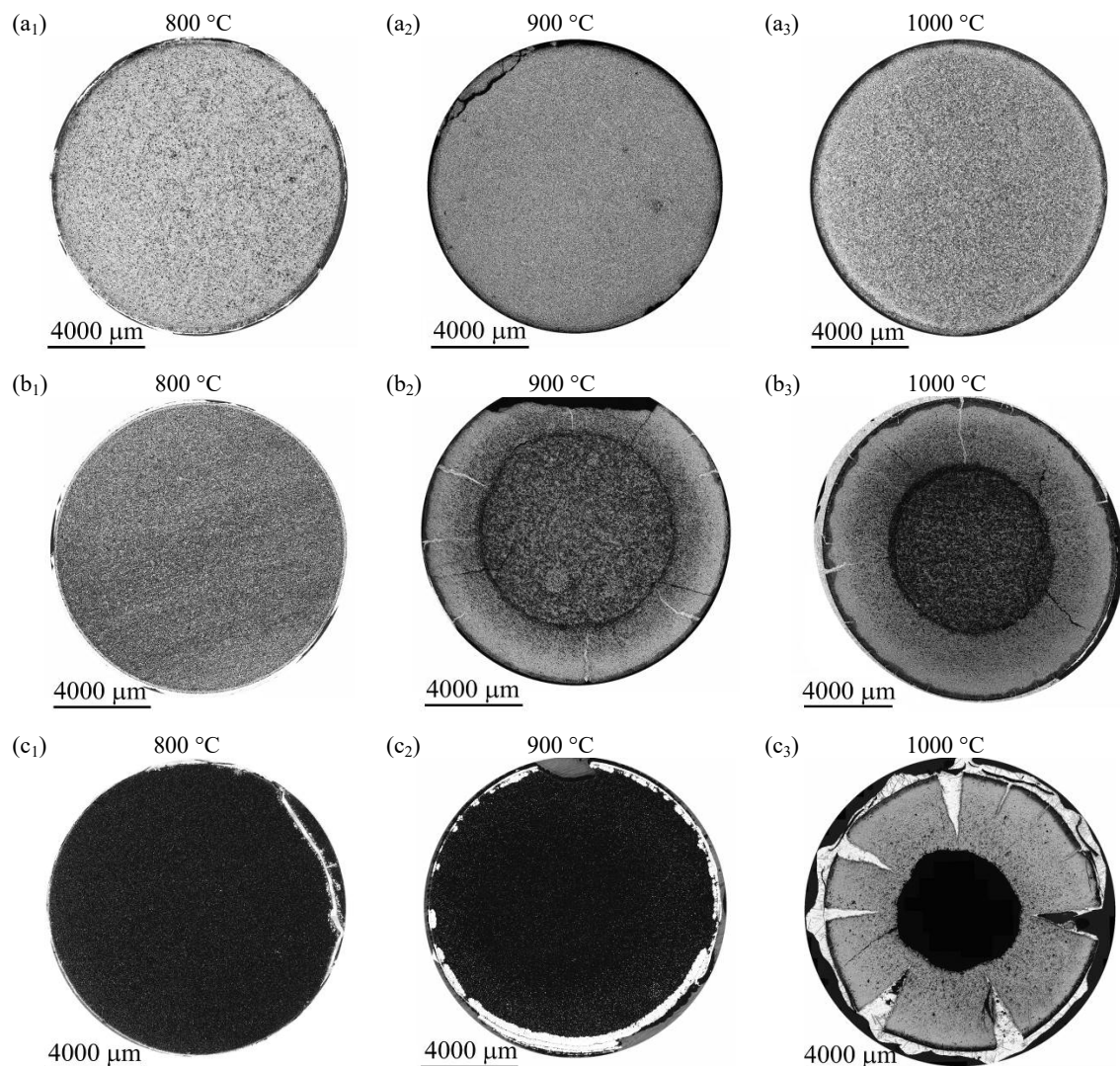


Fig. 6 Cross-sectional panoramas of infiltrated specimens: (a) TiO_2 -70vol.%Al; (b) TiO_2 -50vol.%Al; (c) TiO_2 -30vol.%Al

temperature of 900 and 1000 °C (Fig. 6(b₂) and Fig. 6(b₃), respectively) present an inhomogeneous structure. In these two specimens, a dense outer layer that surrounds a porous inner core is formed, and several radial cracks filled with Al can be noticed in the outer layer. A similar behavior is observed in the TiO₂-30vol.%Al specimens, even if some difference may be outlined. In this case, an outer layer and some radial cracks are observed in the specimens infiltrated at 1000 °C (Fig. 6(c₃)), while only a slight reaction layer is found in 900 °C ones (Fig. 6(c₂)) and neither infiltration nor outer layer are noticed in the 800 °C case (Fig. 6(c₁)).

To explain these structures, it must be considered that in the case of TiO₂-70vol.%Al and TiO₂-50vol.%Al specimens a rather high amount of aluminum is already present in the preform. As shown by XRD analysis, this brings to the formation of a noticeable quantity of TiAl₃, which greatly improves the wettability of the preform and facilitates the successful infiltration. At 800 °C, however, the reaction kinetics is relatively slow, so that while the TiAl₃ phase is formed throughout the sample, infiltration can take place from the outside, filling the voids and bringing to a dense composite.

The same thing does not happen in TiO₂-30vol.%Al specimens at 800 °C, because in this case a lower quantity of the TiAl₃ phase is formed, as shown in the XRD spectrum, due to the lower available quantity of aluminum. The failure in infiltration at 800 °C is generated by the insufficient amount of this phase.

In the case of higher temperature, 900 and 1000 °C, another mechanism takes place instead, since an incomplete infiltration is observed also in the case of TiO₂-50vol.%Al specimens. At these temperatures, it must be considered that the reaction rate increases, and TiAl₃ is formed more rapidly. As shown in Table 2, there is a great increase in the volume of solid phases during the formation of TiAl₃. Consequently, the infiltration paths among the solid phases in the specimens is narrowed or even blocked before the full infiltration can take place, which impedes the infiltration progress. However, since the preform is immersed in a bath of Al alloy, the newly-formed TiAl₃ phase is slowly dissolved by the surrounding Al, and the infiltration is only slowed down and not completely blocked. However, when the surrounding Al bath encounters some unreacted TiO₂ or transitional Ti_mO_n, it generates a local volume increase that brings to radial cracking towards the interior, with the cracks filled by external Al due to the good wettability. The reason why the specimens as shown in Figs. 6(b₂), (b₃), (c₂) and (c₃) are only partially infiltrated is essentially due only to the slowness of the infiltration.

Therefore, it is necessary to control both the TiO₂-to-Al blending ratio and the infiltration temperature in order to obtain a successful spontaneous infiltration.

4 Conclusions

(1) The reaction between TiO₂ and Al was confirmed to happen through a series of reactions with transitional titanium oxides (Ti₂O, TiO, Ti₂O₃ and Ti₃O₅) with lower oxygen content than TiO₂, that were detected during TiO₂-Al reactions in both sintering and infiltration treatment.

(2) TiAl₃ and α -Al₂O₃ were found to be the final products of the reaction in the temperature range of 800–1000 °C, at least in the case of excess of Al.

(3) It was also demonstrated that the sealing of the preform by Al improves the TiO₂-Al reactions with respect to a standard argon atmosphere, where oxide layers and limited wettability can reduce the reaction extent.

(4) Regarding the composites formation, it was demonstrated that the wettability of TiO₂ can be activated by blending with Al, and that the infiltration can be controlled by a convenient choice of both the TiO₂-to-Al blending ratio and the infiltration temperature.

(5) Three main types of microstructures were observed after infiltration: full infiltration, partial infiltration with the formation of cracks and no infiltration. The formation of these microstructures was explained on the basis of reaction kinetics and local volume changes due to the reactions.

(6) It can be said that, to realize an overall good spontaneous infiltration, a TiO₂-to-Al blending ratio around 3:7 in volume and an infiltration temperature around 900 °C are the most suitable.

Acknowledgements

One of the authors, Xiang CHEN, would like to acknowledge the Chinese Scholarship Council (CSC) for financial support (2010612033).

References

- [1] HIRSCH J. Recent development in aluminium for automotive applications [J]. Transactions of Nonferrous Metals Society of China, 2014, 24: 1995–2002.
- [2] SABOORI A, GALLO D, BIAMINO S, FINO P, LOMBARDI M. An overview of additive manufacturing of titanium components by directed energy deposition: Microstructure and mechanical properties [J]. Applied Sciences, 2017, 7(9): 883.
- [3] SHAMSAEI N, YADOLLAHI A, BIAN L, THOMPSON S M. An overview of direct laser deposition for additive manufacturing. Part II:

- Mechanical behavior, process parameter optimization and control [J]. *Additive Manufacturing*, 2015, 8: 12–35.
- [4] PEREZ-BUSTAMANTE R, BOLANOS-MORALES D, BONILLA-MAETINEZ J, ESTRADA-GUEL I. Microstructural and hardness behavior of graphene-nanoplatelets/aluminum composites synthesized by mechanical alloying [J]. *Journal of Alloys and Compounds*, 2014, 615: 578–582.
- [5] DORRI MOGHADAM A, SCHULTZ B F, FERGUSON J B, OMRANI E, ROHATGI P K, GUPTA N. Functional metal matrix composites: Self-lubricating, self-healing, and nanocomposites—An outlook [J]. *The Journal of the Minerals, Metals & Materials Society (TMS)*, 2014, 66: 872–881.
- [6] JAVDANI A, DAEI-SORKHABI A H. Microstructural and mechanical behavior of blended powder semisolid formed Al7075/B₄C composites under different experimental conditions [J]. *Transactions of Nonferrous Metals Society of China*, 2018, 28: 1298–1310.
- [7] TAGHIABADI R, FAYEGH A, PAKBIN A, NAZARI M, GHONCHEH M H. Quality index and hot tearing susceptibility of Al–7Si–0.35Mg–xCu alloys [J]. *Transactions of Nonferrous Metals Society of China*, 2018, 28: 1275–1286.
- [8] SABOORI A, CASATI R, ZANATTA A, PAVESE M, BADINI C, VEDANI M. Effect of graphene nanoplatelets on microstructure and mechanical properties of AISi10Mg nanocomposites produced by hot extrusion [J]. *Powder Metallurgy and Metal Ceramics*, 2018, 56: 647–655.
- [9] SABOORI A, MOHEIMANI S K, DADKHAH M, PAVESE M, BADINI C, FINO P. An overview of key challenges in the fabrication of metal matrix nanocomposites reinforced by graphene nanoplatelets [J]. *Metals*, 2018, 8: 172.
- [10] SABOORI A, PAVESE M, BADINI C, FINO P. Development of Al- and Cu-based nanocomposites reinforced by graphene nanoplatelets: Fabrication and characterization [J]. *Frontiers of Materials Science*, 2017, 11: 171–181.
- [11] ZHU J, WANG F, WANG Y, ZHANG B, WANG L. Interfacial structure and stability of a co-continuous SiC/Al composite prepared by vacuum-pressure infiltration [J]. *Ceramics International*, 2017, 43: 6563–6570.
- [12] SABOORI A, PADOVANO E, PAVESE M, DIERINGA H, BADINI C. Effect of solution treatment on precipitation behaviors, age hardening response and creep properties of Elektron21 alloy reinforced by AlN nanoparticles [J]. *Materials (Basel)*, 2017, 10(12): 1380.
- [13] CUI Y, JIN T, CAO L, LIU F. Aging behavior of high volume fraction SiC_p/Al composites fabricated by pressureless infiltration [J]. *Journal of Alloys and Compounds*, 2016, 681: 233–239.
- [14] SABOORI A, PAVESE M, BADINI C, FINO P. A novel Cu-GNPs nanocomposite with improved thermal and mechanical properties [J]. *Acta Metallurgica Sinica (English Letters)*, 2018, 31: 148–152.
- [15] RASHAD M, PAN F, GUO W, LIN H, ASIF M, IRFAN M. Effect of alumina and silicon carbide hybrid reinforcements on tensile, compressive and microhardness behavior of Mg–3Al–1Zn alloy [J]. *Materials Characterization*, 2015, 106: 382–389.
- [16] SABOORI A, MOHEIMANI S K, PAVESE M, BADINI C, FINO P. New nanocomposite materials with improved mechanical strength and tailored coefficient of thermal expansion for electro-packaging applications [J]. *Metals (Basel)*, 2017, 7(12): 536.
- [17] RASHAD M, PAN F, LIU Y, CHEN X, LIN H, PAN R, ASIF M, SHE J. High temperature formability of graphene nanoplatelets-AZ31 composites fabricated by stir-casting method [J]. *Journal of Magnesium and Alloys*, 2016, 4: 270–277.
- [18] SABOORI A, PAVESE M, BADINI C, FINO P. A novel approach to enhance the mechanical strength and electrical and thermal conductivity of Cu-GNP nanocomposites [J]. *Metallurgical and Materials Transactions A: Physical Metallurgy and Materials Science*, 2018, 49: 333–345.
- [19] AIKIN R M. The mechanical properties of in-situ composites [J]. *The Journal of the Minerals, Metals & Materials Society (TMS)*, 1997, 79: 35–39.
- [20] TJONG S C, MA Z Y. Microstructural and mechanical characteristics of in situ metal matrix composites [J]. *Materials Science and Engineering R: Reports*, 2000, 29: 49–113.
- [21] MAITY P C, CHAKRABORTY P N, PANIGRAHI S C. Processing and properties of Al/Al₂O₃ (TiO₂) in situ particle composite [J]. *Journal of Materials Processing Technology*, 1995, 53: 857–870.
- [22] FENG C F, FROYEN L. Formation of Al₃Ti and Al₂O₃ from an Al–TiO₂ system for preparing in-situ aluminium matrix composites [J]. *Composite Part A: Applied Science and Manufacturing*, 2000, 31: 385–390.
- [23] TRAVITZKY N, GOTMAN I, CLAUSSEN N. Alumina–Ti aluminide interpenetrating composites: Microstructure and mechanical properties [J]. *Materials Letters*, 2003, 57: 3422–3426.
- [24] HORVITZ D, GOTMAN I, GUTMANAS E.Y, CLAUSSEN N. In situ processing of dense Al₂O₃–Ti aluminide interpenetrating phase composites [J]. *Journal of the European Ceramic Society*, 2002, 22: 947–954.
- [25] GHEORGHE I, RACK H J. Reactive infiltration of 25 vol pct TiO₂/Al composites [J]. *Metallurgical and Materials Transactions A*, 2002, 33: 2155–2162.
- [26] GHEORGHE I, RACK H J. Influence of TiO₂/Al ratio on reaction path during reactive infiltration of TiO₂ by molten Al [J]. *Materials Science and Technology*, 2002, 18: 1079–1084.
- [27] PENG H X, WANG D Z, GENG L, YAO C K, MAO J F. Evaluation of the microstructure of in-situ reaction processed Al₃Ti–Al₂O₃–Al composite [J]. *Scripta Materialia*, 1997, 37: 199–204.
- [28] PENG H X, FAN Z, WANG D Z. In situ Al₃Ti–Al₂O₃ intermetallic matrix composite: Synthesis, microstructure, and compressive behavior [J]. *Journal of Materials Research*, 2000, 15: 1943–1949.
- [29] PAN J, LI J H, FUKUNAGA H, NING X G, YE H Q, YAO Z K, YANG D M. Microstructural study of the interface reaction between titania whiskers and aluminum [J]. *Composites Science and Technology*, 1997, 57: 319–325.
- [30] WAGNER F, GARCIA D E, KRUPP A, CLAUSSEN N. Interpenetrating Al₂O₃–TiAl₃ alloys produced by reactive infiltration [J]. *Journal of the European Ceramic Society*, 1999, 19: 2449–2453.
- [31] SABOORI A, PAVESE M, BADINI C, FINO P. Effect of sample preparation on the microstructural evaluation of Al-GNPs nanocomposites [J]. *Metallography, Microstructure, and Analysis*, 2017, 6: 619–622.
- [32] SABOORI A, PAVESE M, BADINI C, FINO P. Microstructure and thermal conductivity of Al-graphene composites fabricated by powder metallurgy and hot rolling techniques [J]. *Acta Metallurgica Sinica (English Letters)*, 2017, 30: 675–687.
- [33] CHEN Z, TAKEDA T, IKEDA K. Microstructural evolution of reactive-sintered aluminum matrix composites [J]. *Composites Science and Technology*, 2008, 68: 2245–2253.

熔融铝对 Al 活化 TiO₂ 的反应自发渗透

Abdollah SABOORI¹, Xiang CHEN^{1,2}, Claudio BADINI¹, Paolo FINO¹, Matteo PAVESE¹

1. Department of Applied Science and Technology, Politecnico di Torino,
Corso Duca Degli Abruzzi 24, 10129 Torino, Italy;

2. Research Center of Graphene Applications, Beijing Institute of Aeronautical Materials, Beijing 100095, China

摘 要: 研究 Al 活化 TiO₂(锐钛矿型)的反应自发渗透。为了进行活化,先将纯 Al 粉与 TiO₂ 混合,再将其压制成预制棒,然后密封于 6060 铝合金模具中。活化和渗透试验在 6060 铝合金浴中完成,时间 1 h。作为对比,在相同的温度和时间条件下,在氩气保护环境中进行烧结试验。X 射线衍射分析表明,就 Al 与 TiO₂ 的反应活化而言,Al 密封环境优于氩气保护。试验发现, TiO₂ 与 Al 的混合比和温度影响渗透和反应动力学,在渗透过程中起着主要的作用。渗透后观察到 3 种主要的显微结构:完全渗透、部分渗透并形成裂纹和无渗透。基于反应动力学和反应导致的局部体积变化,解释这些显微结构的形成原因。最后,研究发现,为了获得总体良好的自发渗透, TiO₂ 与 Al 混合比(体积比)约 3:7、渗透温度约 900 °C 最为适宜。

关键词: 自发渗透; 无压烧结; TiO₂-Al 反应; 渗透动力学; 原位制备

(Edited by Bing YANG)